Effect of stray field on local spin modes in exchange-biased magnetic tunnel junction elements

Effect of stray field on local spin modes in exchange-biased magnetic tunnel junction elements

J. H. H. Rietjens,[a] C. Józsa, W. J. M. de Jonge, and B. Koopmans
Department of Applied Physics, Center for NanoMaterials, Eindhoven University of Technology, P.O. Box 513, 5600 MB Eindhoven, Netherlands

H. Boeve
Philips Research Laboratories, Prof. Holstlaan 4, 5656 AA Eindhoven, Netherlands

(Received 17 May 2005; accepted 30 August 2005; published online 20 October 2005)

We report on the detection of localized spin modes in a multilayered spintronic device by means of time-resolved scanning Kerr microscopy. Measurements on this 13×9 μm^2 exchange-biased magnetic tunnel junction element at different applied bias fields indicate a strong effect of the stray field from the pinned CoFe layer on the magnetization dynamics in the free NiFe layer. This view is supported by micromagnetic simulations, which also show that the dynamics can be attributed to the specific shape of the internal magnetic field in the element. © *2005 American Institute of Physics*. [DOI: 10.1063/1.2117614]

Magnetic tunnel junction (MTJ) elements are currently being implemented in spintronic devices, such as magnetic random access memory.[1,2] Switching of the magnetization in the free ferromagnetic (FM) layer of a MTJ can be achieved by applying an external magnetic field (pulse),[3] and has to be fast and stable. Understanding the response of the magnetization in the free layer to an applied magnetic field (pulse) is therefore crucial for obtaining an optimal performance of the device. In recent years, the magnetization dynamics in relatively thick NiFe stripes and elements has been the subject of many studies,[4–8] but so far no measurements on MTJs have been reported. In this letter, we present spatiotemporal measurements and micromagnetic simulations of the magnetization dynamics in the free FM layer of an exchange-biased MTJ element. We show that this dynamic is strongly influenced by the stray field, H_{stray}, from the pinned FM layer of the MTJ.

The MTJ element studied in this work was grown by sputter deposition and structured by etching, see Figs. 1(a) and 1(b). The Cu strip line (width 30 μm, thickness 17 nm) with contact pads at each end was deposited on a Si/SiO_2 substrate. The 13×9 μm^2 MTJ element, located at the center of the Cu line, consists of Ta and NiFe wetting layers, followed by an (IrMn 10 nm/$Co_{90}Fe_{10}$ 4 nm/Al_2O_3 1 nm/$Ni_{80}Fe_{20}$ 5 nm) stack and a 5 nm Ta capping layer. superconducting quantum interference device measurements showed an exchange bias field of 31 kA/m acting on the CoFe layer and a 5 kA/m net FM coupling field H_{FM} between the NiFe and the CoFe layer. The direction of the exchange bias field (and thus the direction of H_{FM}) was set along the Cu line (x direction) by an in-field anneal treatment.

The magnetization dynamics is triggered by magnetic field pulses $H_{pulse}(t)$ of ~0.6 ns with $H_{pulse,max}\approx1.2$ kA/m. These pulses are generated with an electronic pulse generator that is connected to the Cu line. The response of the magnetization in the free FM layer to such field pulses is typically a damped precessional motion. The local out-of-plane component of this response, $m_z(\mathbf{x},t)$, is probed with time-resolved scanning Kerr microscopy, which is described in detail in Ref. 9. An example of a time-resolved measurement is shown in Fig. 1(c).

Micromagnetic simulations of the magnetization dynamics were performed using the Object-Oriented MicroMagnetic Framework (OOMMF).[10] The MTJ element is divided into a two-dimensional grid of 25 nm×25 nm×5 nm cells. Reduction of the cell size gave no different results. The material parameters used for the NiFe layer are $M_{s,NiFe}=570$ kA/m, $\alpha=0.01$, $A=13\times10^{-12}$ J/m, where M_s is the saturation magnetization, α the Gilbert damping parameter, and A the exchange stiffness. The dc magnetic field in the simulation is the sum of the experimentally applied bias field H_{bias} and 5.0 kA/m representing H_{FM}. A magnetic field pulse with shape similar to the real pulse (rise/fall time 0.25 ns,

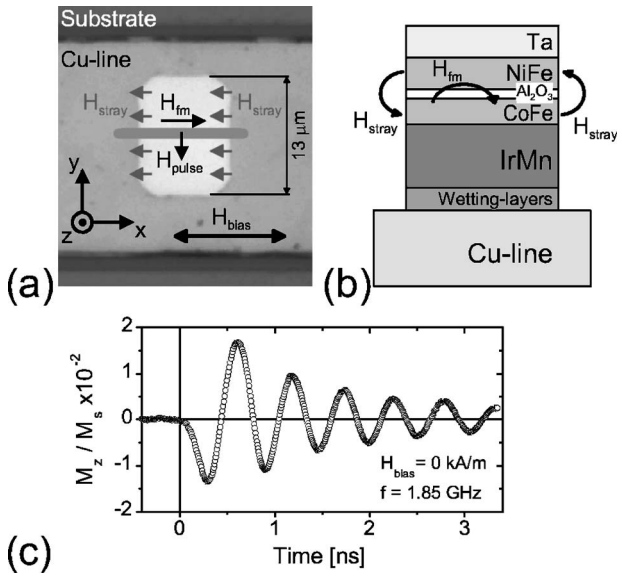

FIG. 1. (a) Photograph of the 13×9 μm^2 MTJ studied in this work. Indicated are the coordinate system, the scanning line of Fig. 3 (gray), and the direction of H_{bias}, H_{pulse}, H_{FM}, and H_{stray}. (b) Schematic cross section of the MTJ. (c) Typical measurement of $m_z(t)$ taken at the center of the MTJ at zero-bias field. A damped precessional motion with frequency 1.85 GHz can be observed.

[a]Electronic mail: J.h.h.rietjens@tue.nl

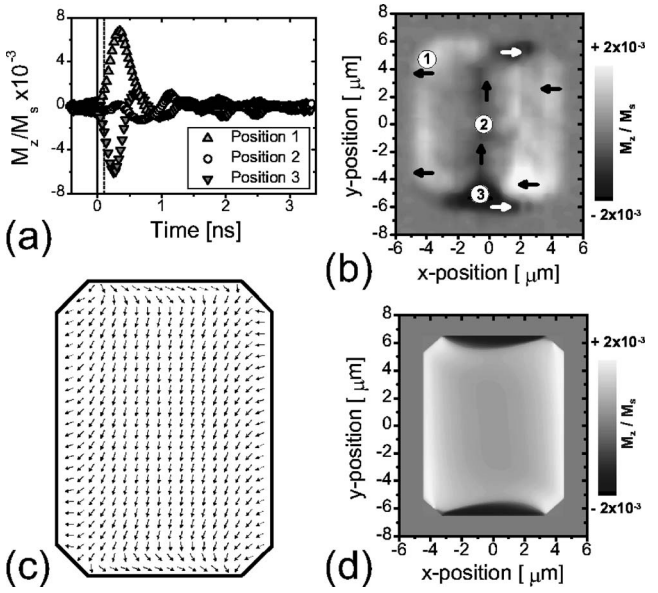

FIG. 2. (a) Three measurements of the response of m_z to H_{pulse} at an external bias field of 5.0 kA/m. The numbered positions correspond to the positions indicated in (b). (b) Image of $m_z(\mathbf{x},t=0.1\text{ ns})$. The arrows indicate the main component of the local in-plane magnetization. (c) Simulated equilibrium magnetization of the MTJ with $H_{\text{bias}}=5.0$ kA/m. (d) Simulated image of $m_z(\mathbf{x},t=0.1\text{ ns})$.

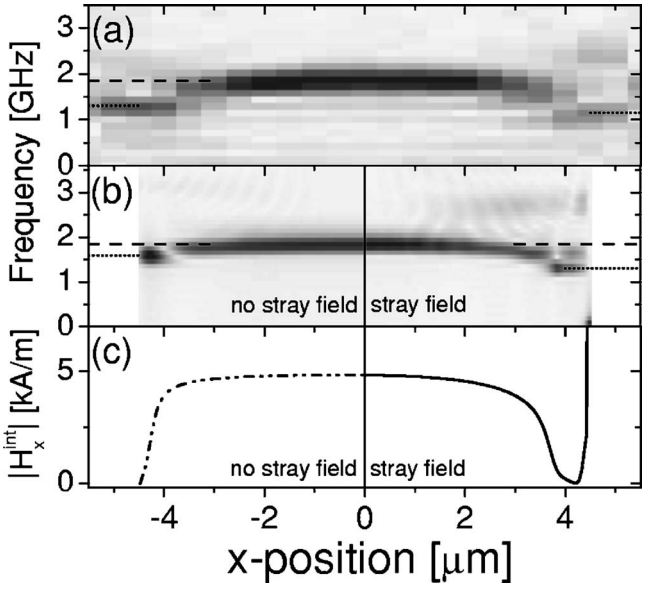

FIG. 3. (a) Experimental spectral image of the line scan in the x direction with $H_{\text{bias}}=0$ kA/m. (b) Simulated spectral image of the experiment of (a), without and with incorporation of a stray field. The gray scale in (a) and (b) represents the spectral power of the frequencies in $m_z(t)$, which is normalized at each position. The frequencies of the uniform (localized) modes are indicated with a dashed (dotted) line. (c) The magnitude of the internal magnetic field without and with stray field. The left- and right-hand side parts of (b) and (c) are symmetric in x.

plateau 0.1 ns) is used to excite the spin system. The response to this field pulse is calculated with a time step of 1 ps.

Let us first consider the experimental case with $H_{\text{bias}}=-5.0$ kA/m, i.e., the case when H_{FM} is fully compensated. The domain pattern in the free NiFe layer will then be the result of the interplay between the demagnetizing field H_{dem}, shape or crystalline anisotropy H_{ani}, and any remaining magnetic influence from the pinned layer. In this situation, no clear precessional motion of $m(\mathbf{x},t)$ could be observed in time-resolved measurements [as can be seen in Fig. 2(a)], so no frequency analysis could be performed. Instead, we used the sign of $m_z(\mathbf{x})$ shortly after application of $H_{\text{pulse}}(t)$ to determine the static domain pattern $m(\mathbf{x},t=0)$, as this sign is related to the orientation of $m(\mathbf{x},t=0)$ by a torque equation, i.e., the well-known Landau–Lifshitz equation.[11] At Position 1, e.g., the sign of $m_z(t=0.1\text{ ns})$ is positive, which implies that $m(t=0)$ at Position 1 has a large component in the negative x direction, since the effective field, $H_{\text{eff}}\approx H_{\text{pulse}}$, is in the $-y$ direction. Similarly, a raster scan of the full element, taken at $t=0.1$ ns after the onset of the magnetic field pulse, reveals the domain pattern in the free layer, as shown in Fig. 2(b). Notably, the magnetization is not aligned along the left- and right-hand side edges, in spite of the demagnetizing field. This suggests a contribution of the stray field H_{stray} from the pinned CoFe layer.

In order to investigate this, micromagnetic simulations of the experiment were performed with the incorporation of H_{stray}. For this purpose, at each cell, H_{stray} is calculated using the formula for the field of a uniformly magnetized element,[12] with $M_{s,\text{CoFe}}=1467$ kA/m, the bulk M_s value of CoFe.[13] The distance between the CoFe layer and the cells is set to 2.5 nm. The equilibrium magnetization of the free layer, after relaxing from a fully magnetized state, is shown in Fig. 2(c). The spins at the left/right-hand side edges are indeed oriented perpendicular to the edge, as a result of H_{stray}. Due to a small anisotropy present in the element (experimentally observed and included in the simulation), the magnetization is aligned along the y axis in the center of the element. Applying H_{pulse} to the initial magnetization state of Fig. 2(c), and calculating $m_z(\mathbf{x},t=0.1\text{ ns})$, results in the image shown in Fig. 2(d). A fair agreement between experiment and simulation can be observed, particularly with respect to the white (black) regions at the left/right (top/bottom) edges and the grey central region. These features are signs of the competition between the H_{stray}, H_{dem}, and H_{ani}. The difference in shape and position of the black regions between experiment and simulation is probably due to the absence of pinning centers in the simulation. These pinning centers are likely to be present in the real MTJ, e.g., due to edge roughness.

When H_{bias} is set to 0 kA/m, the internal field at the center of the element is ~5.0 kA/m. In this case, a precessional motion of $m_z(\mathbf{x},t)$ can be observed, which allows for a frequency analysis. Therefore, $m_z(\mathbf{x},t)$ has been measured locally along the x direction through the center of the element, see Fig. 1(a). Each measurement of $m_z(t)$ is taken at fixed positions of the laser spot on the sample, in steps of 0.5 μm. The resulting Fourier transformation of $m_z(\mathbf{x},t)$ at each position is shown in Fig. 3(a). A uniform precessional mode can be observed roughly from −3.5 to +3.5 μm, with a frequency, f_{uni}, that decreases from 1.85 GHz to 1.76 GHz when moving from 0 to ±3.5 μm. At the edges of the element, a localized mode with $f_{\text{loc}}\approx 1.3$ GHz can be clearly seen. At +4 μm, a higher-order mode is also observed.

It has been shown,[4,5] that such remarkable localized modes can occur in a region where the internal magnetic field, H_{int}, is highly inhomogeneous. Such a region can arise near the edge of an element due to the demagnetization field, when an external field [or coupling field (H_{FM}) as in our experiment] is perpendicular to the edge. Spin waves propa-

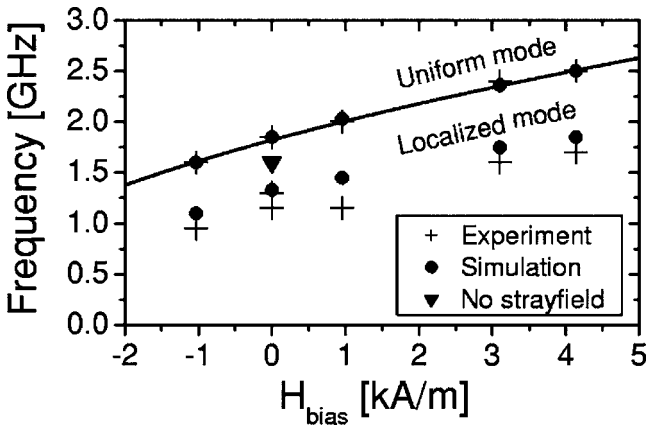

FIG. 4. The frequency of the uniform and localized mode (experiment and simulation) as a function of the externally applied bias field. At 0 kA/m are shown the frequencies of the localized modes at both sides of the element (experimental) and from the simulation when no stray field is incorporated. The solid curve is the theoretical frequency of the uniform mode.

gating parallel to this field become confined in a potential well created by the inhomogeneous internal magnetic field, leading to a localized mode. The frequency of the localized mode depends on the precise shape of the potential well.

We performed micromagnetic simulations in order to calculate the frequency of the localized mode. The result of this simulation, without and with incorporation of H_{stray}, is shown in Fig. 3(b). The frequency of the uniform mode agrees well with the experiment in both simulations. However, both the gradual decrease of f_{uni} when moving from the center to the edge, and f_{loc} agree only in the case when H_{stray} is included. This can be understood by looking at the internal magnetic field in the element, see Fig. 3(c). The steep increase in H_{int} at ~ 4.5 μm [Fig. 3(c) right-hand side part] is due to the strong stray field close to the magnetic pole of the CoFe layer. The gradual decrease of H_{int} between 0 and 3 μm is also due to the contribution of the stray field and results in the gradual decrease f_{uni}. Furthermore, H_{int} clearly behaves differently in the region where the localized mode is present, which results in a different shape of the potential well and a ~ 0.3 GHz lower frequency of the localized mode. Around +4 μm, the simulated spectrum shows multiple peaks that do not correspond directly to the ones observed in the experiment. This fact, and the lack of symmetry in the experimental data (there is a 0.15 GHz difference between f_{loc} at the left- and right-hand side edge of the element) in contrast to the simulations, can be attributed to a slight difference in the internal magnetic field near the edges, as a result of sample imperfections.

We also measured and simulated f_{uni} and f_{loc} at different bias fields, as presented in Fig. 4. A good agreement between experiment, simulation, and theory can be observed for the uniform mode, which depends on H_{bias} according to $f_{\text{uni}} = \gamma\mu_0\sqrt{(H_{\text{bias}}+H_{\text{FM}})(H_{\text{bias}}+H_{\text{FM}}+M_s)}$, where γ is the gyromagnetic ratio and μ_0 is the magnetic permeability of vacuum. The dependence of f_{loc} on H_{bias} is similar to the one in the experimental case, but their absolute values are on average ~ 0.16 GHz higher. This difference is comparable to the differences attributed to sample imperfections, so a satisfactory agreement between experiment and simulation is found when the stray field is included. Moreover, using a more realistic stray field, based on, e.g., a nonuniformly magnetized CoFe layer, might even improve these results.

In conclusion, the experimental data and the simulations indicate a strong effect of the stray field from the pinned CoFe layer on the properties of the free NiFe layer. Most pronounced effects are the orientation of the magnetization at the edges when H_{FM} is compensated, and the low-frequency localized modes when H_{FM} is uncompensated. These observations can be explained by the specific shape of internal magnetic field in the element. In view of applications, it is necessary to reduce the effect of the stray field as much as possible. This will be specifically relevant when the size of the MTJ's is reduced to below 1 μm. Coherent precessional switching, e.g., may become impossible due to the presence of localized modes near the edges of the element.

This work is supported by NanoNed, a nanotechnology program of the Dutch Minister of Economic Affairs, and part of the research program of FOM, which is financially supported by NWO.

[1] S. A. Wolf, D. D. Awschalom, R. A. Buhrman, J. M. Daughton, S. von Molnár, M. L. Roukes, A. Y. Chtchelkanova, and D. M. Treger, Science **294**, 1488 (2001).
[2] B. N. Engel, J. Akerman, B. Butcher, R. W. Dave, M. DeHerrera, M. Durlam, G. Grynkewich, J. Janesky, S. V. Pietambaram, N. D. Rizzo, J. M. Slaughter, K. Smith, J. J. Sun, and S. Tehrani, IEEE Trans. Magn. **41**, 132 (2005).
[3] H. W. Schumacher, C. Chappert, R. C. Sousa, P. P. Freitas, and J. Miltat, Phys. Rev. Lett. **90**, 017204 (2003).
[4] J. Jorzick, S. O. Demokritov, B. Hillebrands, M. Bailleul, C. Fermon, K. Y. Guslienko, A. N. Slavin, D. V. Berkov, and N. L. Gorn, Phys. Rev. Lett. **88**, 047204 (2002).
[5] J. P. Park, P. Eames, D. M. Engebretson, J. Berezovksy, and P. A. Crowell, Phys. Rev. Lett. **89**, 277201 (2002).
[6] A. Barman, V. V. Kruglyak, R. J. Hicken, and J. M. Rowe, Phys. Rev. B **69**, 174426 (2004).
[7] M. Buess, R. Höllinger, T. Haug, K. Perzlmaier, U. Krey, D. Pescia, M. R. Scheinfrein, D. Weiss, and C. H. Back, Phys. Rev. Lett. **93**, 077207 (2004).
[8] K. Perzlmaier, M. Buess, C. H. Back, V. E. Edimov, B. Hillebrands, and S. O. Demokritov, Phys. Rev. Lett. **94**, 057202 (2005).
[9] J. H. H. Rietjens, C. Józsa, H. Boeve, W. J. M. de Jonge, and B. Koopmans, J. Magn. Magn. Mater. **290**, 494 (2005).
[10] M. J. Donahue and D. G. Porter, OOMMF User's Guide, version 1.0, Interagency Report NISTIR 6376, NIST ⟨http://math.nist.gov/oommf⟩
[11] L. Landau and E. Lifshitz, Phys. Z. Sowjetunion **8**, 153 (1953).
[12] J. D. Jackson, *Classical Electrodynamics*, 3rd ed. (Wiley, New York, 1999), pp. 196–197.
[13] Landolt-Börnstein, *Group III Condensed Matter* (Springer, Berlin, 1986), Vol. 19a, p. 189.